Lubrication of Highly Viscous Core-Annular Flows in Microfluidic Chambers

Samira Darvishi

Thomas Cubaud[1]
e-mail: thomas.cubaud@stonybrook.edu

Department of Mechanical Engineering,
Stony Brook University,
Stony Brook, NY 11794

We investigate the lubrication transition of high-viscosity fluid threads flowing in sheaths of less viscous fluids, i.e., viscous core-annular flows, in microchannels. Focus is given on the flow behavior of threads as they traverse a quasi-two-dimensional diverging-converging slit microfluidic chamber. The role of the viscosity contrast is examined for both miscible and immiscible fluids, and, for the later case, both partially wetting and nonwetting threads are considered. The conditions for lubrication are established in relation to flow rates of injection, interfacial properties, viscosities, and phenomena such as viscous buckling, wetting, breakup, and coalescence. [DOI: 10.1115/1.4003733]

1 Introduction

The manipulation of highly viscous materials at the microscale is a key challenge for implementing lab-on-chips with the ability to manage a variety of complex and reactive fluids. Microfluidic platforms offer great opportunities for controlling multifluid flows and interfaces at the small scale. The unique behavior of microflows finds applications in many fields of interests [1–3] and facilitates studies of fast reactions, biomedical detection and diagnostics, environmental monitoring, and micropower generation [4–8]. The manipulation of fluid interfaces is important for the development of optofluidic elements, including lenses and waveguides [9–11], as well as for sequestrating reactive components into individual droplets and bubbles [12–14]. Motivated by this vast array of applications, the continuous formation of bubbles and droplets has been extensively studied in a variety of microgeometries [15–20].

A broad range of industrial and biological fluids are highly viscous and their manipulation at the small scale would provide new facilities for lab-on-chip devices. Most microfluidic studies, however, have been conducted using fluids that exhibit a relatively low-viscosity coefficient. As the dimension shrinks, the hydraulic resistance significantly increases and many of the early microflow investigations have focused on low-viscosity fluids to mitigate the large pressure drop required to displace fluids in confined microsystems. A promising strategy for precisely handling "thick" fluids involves the formation of a highly viscous fluid core lubricated by a less viscous fluid, i.e., a viscous core-annular flow or a viscous thread [21–23]. The self-lubrication property of fluids having a large difference in viscosities [24,25] has been relatively unexplored at the small scale. In addition to its application to fluid transport in narrow geometries and porous media, characterizing the evolution of viscous stratifications is also important for designing novel continuous flow reactors between soft materials and solvents.

Here, we examine the behavior of viscous threads flowing in a quasi-two-dimensional pore. A diverging-converging microfluidic chamber is connected with two microchannels that are square in cross section and are used as the fluid inlet and outlet. In a diverging microchannel, a viscous thread experiences a flow rate-controlled folding instability [21]. Slender viscous structures are known to buckle in a fashion similar to elastic solids during short intervals of time [26–29]. In this work, we show that the folding instability can be exploited for the interfacial control of high-viscosity fluids. Our microfluidic cell is advantageous for investigating the role of fluid properties and flow parameters on the stability of viscous core-annular flows. This study aims at forging a unifying picture between miscible and immiscible fluid microthreads.

First, we discuss the behavior of miscible threads as this regime yields insight on the influence of the viscosity contrast between liquids. Flow morphologies are analyzed and the dramatic lubrication failure of weakly diffusive threads on the top and bottom walls of the chambers is characterized. Second, the behavior of core-annular flows formed between two immiscible liquids is examined. In this situation, the non-negligible interfacial tension between fluids and the wetting properties of the thread at the walls play an important role on flow architectures. Using different fluid pairs, this system is studied for a nonwetting thread and for a partially wetting thread. Novel combinations of viscous and capillary instabilities are shown to offer innovative mechanisms for manipulating the lubrication properties of high-viscosity fluids in confined microdomains.

2 Microfluidic Chambers

Hard microfluidic modules made of silicon and glass were fabricated. A double-sided polished silicon wafer ($h=100$ μm or 250 μm) is etched-through using DRIE and then sealed between two flat borosilicate glass plates using anodic bonding [30]. To visualize flows, the module is placed onto an inverted microscope with a fiber light on top to provide enough illumination for high-speed imaging. Fluids are injected into the channel with high-pressure syringe pumps.

The microfluidic platform consists of two sections, a hydrodynamic focusing section to create the thread and a square-shaped diverging-converging chamber (Fig. 1(a)). First, a viscous thread is produced in the focusing section. The more viscous liquid ($L1$) having a viscosity η_1 is introduced in the central channel at a flow rate Q_1 and the less viscous fluid ($L2$) having a viscosity η_2 is symmetrically injected in the side channels with a total flow rate Q_2. This simple method permits the formation of a viscous core (i.e., viscous thread) made of $L1$ lubricated by the less viscous fluid $L2$ in the square microchannel that leads to the chamber. In previous studies [21–23], we found that for large viscosity ratios $\chi=\eta_1/\eta_2>15$, the thread diameter normalized by the channel height ε/h depends only on the flow rate ratio $\varphi=Q_1/Q_2$ according to $\varepsilon/h=(\varphi/2)^{1/2}$. This scaling is useful to describe the shape of a viscous thread both in miscible environments for $Pe>10^3$, where the Péclet number is $Pe=hV/D$ with V being the average

[1]Corresponding author.

Contributed by the Fluids Engineering Division of ASME for publication in the JOURNAL OF FLUIDS ENGINEERING. Manuscript received December 17, 2010; final manuscript received February 23, 2011; published online March 29, 2011. Assoc. Editor: Neelesh A. Patankar.

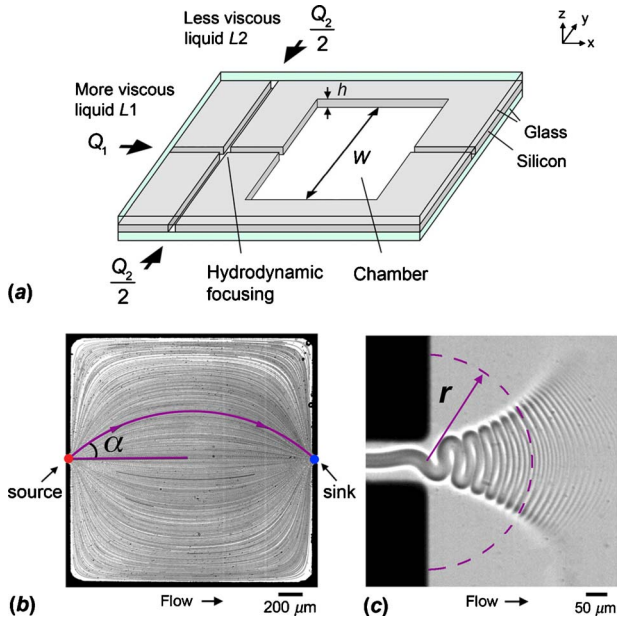

Fig. 1 Microfluidic chamber: (*a*) schematic of microchannel layout, (*b*) single-phase flow streamlines, and (*c*) folding morphology at the chamber inlet

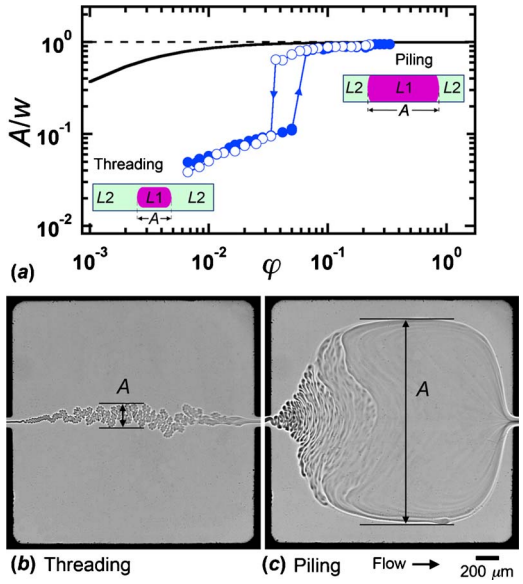

Fig. 2 Lubrication failure of a viscous thread for χ=592. (*a*) Hysteresis loop between threading and piling regimes: increasing φ (●) and decreasing φ (○). Solid line: $A/w=[1+(\chi\varphi)^{-1}]^{-1}$. Experimental pictures with flow rates (μl/min): (*b*) Q_1=2 and Q_2=110 and (*c*) Q_1=5 and Q_2=40.

flow velocity and D being the molecular diffusion coefficient, and in immiscible surroundings when $Ca_1 > 10^{-1}$, where $Ca_1 = \eta_1 Q_1/(\gamma_{12} h^2)$ is the capillary number associated with the injection flow rate of the more viscous fluid and γ_{12} is the interfacial tension between $L1$ and $L2$.

Downstream from the square channel, the thread and ensheathing fluid enter the chamber that is characterized by a large width-to-height aspect ratio $w/h=20$. The large aspect ratio of the chamber allows for comparing flow behavior with a Hele–Shaw cell approximation [31]. In such a cell, a single-phase flow can be considered as irrotational and the streamlines of steady flows are expected to be identical in shape with those of an inviscid fluid [32]. To investigate this aspect, the flow was seeded with 2 μm-diameter spheres and consecutive images were superimposed to form a composite picture (Fig. 1(*b*)). This method, which is equivalent to a long exposure photograph, reveals streamlines and shows that the inlet channel flow can be described as a source and the outlet channel flow as a sink. In the center of the cell, i.e., away from the sidewalls, streamlines can be roughly approximated by circular arcs identified by their initial angle α. This analysis suggests that, in the first section of the chamber, the mean flow velocity $V \propto 1/r$, with r being the distance from the source, and equipotential lines are expected to be circular. This effect is also observed for multiphase flows. For instance, a deformed thread advected in the diverging flow field of $L2$ displays nearly circular folding lines having a radius of curvature r (Fig. 1(*c*)).

Overall, our microfluidic chamber can be viewed as a simple fluidic element that allows for manipulating threads and high-viscosity liquids. Such flow geometry, which we have previously labeled as "a microfluidic aquarium" [33], is particularly well suited for interrogating the influence of fluid properties on micro-multiphase flows.

3 Miscible Viscous Core-Annular Flows

Miscible viscous core-annular flows are studied using conventional silicone oils (i.e., polydimethylsiloxane (PDMS) oils) having a wide range of viscosity: $0.82 \leq \eta \leq 4865$ cP. These polymeric oils are fully miscible and considered Newtonian in the range of shear rates γ presently investigated ($\gamma < 10^3$ s^{-1}). Provided that the Péclet number is large enough ($Pe > 10^3$), the effects of molecular diffusion are weak. Using miscible fluids in the weakly diffusive regime is helpful for investigating the influence of the viscosity ratio χ in the absence of the complicated effects due to interfacial tension and wetting phenomena. Since the initial thread size ε does not depend on χ nor interfacial properties in the inlet square channel, we can finely control the initial conditions and examine the role of fluid properties and flow parameters in the chamber.

The thread formed in the hydrodynamic focusing section begins to fold as it enters the chamber (Fig. 1(*c*)). The folds define an envelope that typically increases in amplitude A in the first part of the chamber (diverging section) and decreases in the second part (converging section) (Figs. 2(*b*) and 2(*c*)). Two regimes are observed: (1) small threads that can traverse the chamber while being lubricated by $L2$ at the top and bottom walls and (2) large threads that make direct contact with the top and bottom walls. The latter situation is characteristic of a lubrication failure and we call the central region "pile," similar to parallel viscous flows [34].

The average envelope amplitude normalized by the chamber width A/w was measured as a function of the flow rate ratio $\varphi = Q_1/Q_2$ (Fig. 2(*a*)). For large viscosity ratios χ, the transition between the two regimes is characterized by an abrupt variation in the envelope amplitude A. This transition depends on the history of the system. We have investigated the hysteresis in the transition by comparing the amplitude A between a system initially in the threading regime and increasing φ (i.e., increasing the initial thread diameter ε) with a system initially in the piling regime and decreasing φ (i.e., decreasing ε). Data show that near the transition, the system can choose different configurations while in the well-defined threading and piling regimes, hysteresis is negligible. In Fig. 2(*a*), we have plotted the expected viscous parallel flow approximation [34] $A/w=[1+(\chi\phi)^{-1}]^{-1}$, which asymptotically matches data for large A. Hysteretic effects can alter the critical flow rate ratio φ_c for the thread lubrication failure by a factor 2. This uncertainty in the transition, however, is relatively small compared with the range of variation of φ that spans over two orders of magnitude.

A comprehensive series of experiments was conducted by systematically varying the viscosity ratios χ (Fig. 3). To focus on the

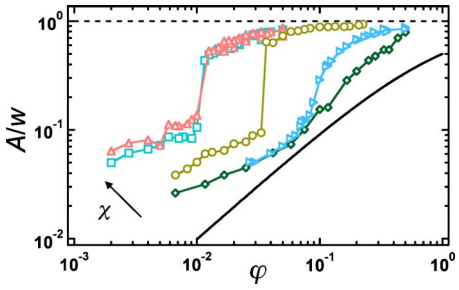

Fig. 3 Evolution of the amplitude A for $\chi=52$ (◇), 106 (▷), 592 (○), 2796 (□), and 5933 (△). Solid line: $A/w=[1+\varphi^{-1}]^{-1}$.

behavior of weakly diffusive threads, data are only shown for cases where the initial thread size decreases and the Péclet number is large ($Pe>10^3$). Indeed, for small flow rates, molecular diffusion blurs the interface and can also significantly alter the transition. As the viscosity ratio χ decreases, the lubrication transition becomes smoother and occurs at a larger flow rate ratio φ. This behavior is related to the ability of a thread to bend in a viscous environment. In general, the thread folding amplitude A increases with the viscosity ratio χ. The smooth transition at low χ is interpreted as a partial lubrication failure. The system can readily integrate the two states (threading and piling) for low χ because the thread is relatively less viscous and therefore can "reflow" in the pile. For comparison, the Hele–Shaw cell approximation for $\chi=1: A/w=[1+\varphi^{-1}]^{-1}$ was plotted. Upon carefully examining the transition for numerous flow rates and viscosity ratios, we define the lubrication transition to occur when $A/w\approx 0.3$, which, given our channel geometry ($w/h=20$), corresponds to $A\approx 6h$.

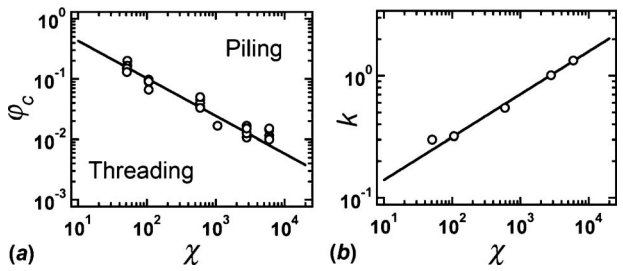

Fig. 4 Influence of viscosity contrast χ. (*a*) Critical flow rate ratio φ_c for lubrication transition. Solid line: $\varphi_c=1.8\chi^{-0.62}$. (*b*) Evolution of the prefactor k. Solid line: $k=0.06\chi^{0.35}$.

The critical flow rate ratio φ_c corresponding to the lubrication transition (i.e., when $A/w\approx 0.3$) was measured for a broad range of χ (Fig. 4(*a*)). Although for each χ, the transition can vary due to the complex interplay between folding and diffusion near the solid surfaces, experiments show that φ_c decreases with χ. We fit our data with a power law and find that the function $\varphi_c=1.8\chi^{-0.62}$ compares well with experimental behavior. The coefficient −0.62 is very close to $-2/3$ and this simple functional relationship is useful for predicting the lubrication failure of a viscous thread in the chamber as a function of χ. In particular, relating φ and ε indicates that the critical initial size ε_c for a thread to traverse the chamber without piling decreases with the viscosity ratio χ.

The influence of χ was also examined in the threading regime. Since the diameter of a lubricated thread in a square channel follows $\varepsilon/h=(\varphi/2)^{1/2}$, by extension, we fit the amplitude of a lubricated folded thread in the chamber with $A/w=k\varphi^{1/2}$. The prefactor k is a function of the viscosity ratio, as can be seen in Fig. 4(*b*). Data are reasonably well fit by the function $k=0.06\chi^{0.35}$, which yields the estimate $A/w\approx c\chi^{1/3}\varphi^{1/2}$ with $c=0.06$. This result shows that although folding morphologies are rather intricate due to primary and secondary folding [34], the mean behavior of the system can be described using scaling laws.

Two parameters are introduced to quantify the shape of the more viscous central layer in the chamber. The first criterion is the penetration length X_P of the lubricated thread into the pile. At the chamber entrance, the thread is lubricated and deposits $L1$ into the slow moving pile. The location of this transition can be estimated

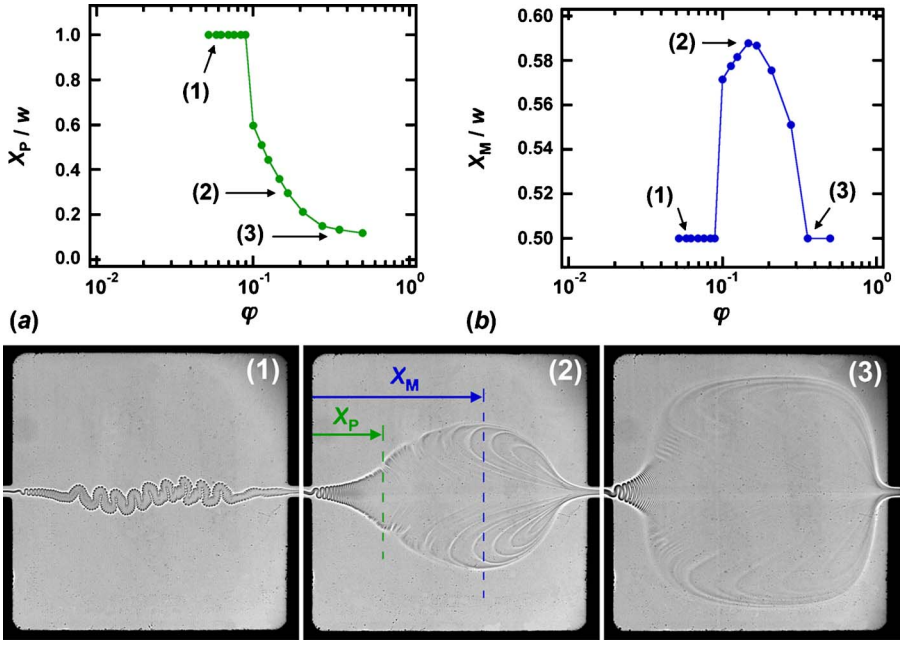

Fig. 5 Morphological features of folding threads ($\chi=106$). (*a*) Apparent penetration length of lubrication X_P/w as a function of flow rate ratio φ. (*b*) Location of maximum amplitude X_M/w for various φ. Bottom: corresponding experimental micrographs ($h=100$ μm, flow rates in μl/min): (1) $Q_1=10$ and $Q_2=180$, (2) $Q_1=7$ and $Q_2=40$, and (3) $Q_1=5$ and $Q_2=14$.

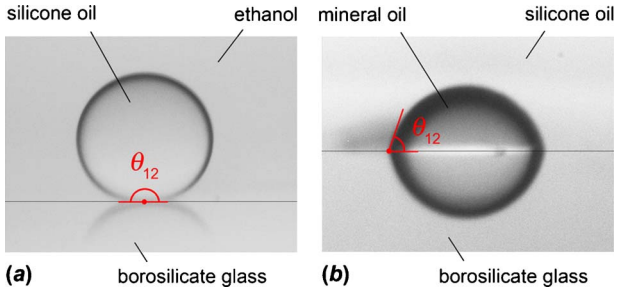

Fig. 6 Liquid/liquid contact angle measurements on borosilicate glass. (*a*) *L*1: silicone oil, *L*2: ethanol, and $\theta_{12}\approx 180$ deg. (*b*) *L*1: heavy mineral oil, *L*2: silicone oil, and $\theta_{12}\approx 70$. Droplets are reflected on the glass surface.

from experimental micrographs by examining the regions where folds start to disappear into the pile. This transition also corresponds to the inversion of the envelope curvature of the central stream (Fig. 5). Thus, when $X_P/w=1$, the thread remains lubricated along the chamber. Smaller penetration length $X_P/w<1$ indicates that the pile has formed. For low χ, we systematically observe that the pile forms near the end of the chamber. Increasing the flow rate ratio φ results in a pile formation in the upstream direction. The assumption that X_P/w decreases with φ is confirmed experimentally (Fig. 5(*a*)).

The second criterion is the location of the maximum central stream amplitude X_M. The lubrication failure is associated with an increase of the amplitude A to conserve mass due to the reduction in the stream velocity resulting from the contact of the more viscous liquid $L1$ with the walls. Therefore, the location of the maximum amplitude X_M indicates where the center of the pile is positioned. For a lubricated thread, the maximum is expected in the center of the chamber, where $X_M/w=0.5$, according to the single-phase streamlines. The center of a fully formed pile is also expected in the middle of the chamber. During the transition, however, X_M appears to shift toward the chamber outlet, as displayed in Fig. 5(*b*). The two parameters X_P and X_M are useful indicators of the smooth lubrication transition for low χ.

4 Immiscible Viscous Core-Annular Flows

The behavior of immiscible viscous core-annular flows can considerably differ from their miscible counterparts due to the effects of wetting and interfacial tension. The stability of the thin lubricating film of $L2$ between the thread and the walls is strongly affected by the surface energies between the solid wall and the fluids, which, in turn, determine the contact angle θ_{12} that is defined with respect to the fluid thread. Overall, wetting is important for the film stability and interfacial tension γ_{12} alters buckling morphologies. The viscous folding process typically increases the thread specific area while interfacial tension forces tend to reduce interfacial area. Hence, immiscible threads in chambers are subjected to two competing mechanisms, namely, the viscous folding and the capillary instabilities.

Microflows are examined in two situations: (a) for a nonwetting thread and (b) for a partially wetting thread. Fluid pairs were selected according to their mutual contact angle on borosilicate glass. For the nonwetting case, we used a silicone oil having a viscosity $\eta_1=485$ cP for $L1$ and ethanol for $L2$ ($\eta_2=1.16$ cP). The contact angle in this situation approaches $\theta_{12}\approx 180$ deg and a drop of $L1$ immersed in a continuous phase of $L2$ assumes a typical bead shape on the glass surface (Fig. 6(*a*)). Using the combined capillary rise method [35] with well-characterized borosilicate glass tubes, we measure the interfacial tension $\gamma_{12}=1.7\pm 0.2$ mN/m between $L1$ and $L2$. For the wetting case, we use a heavy mineral oil having a viscosity of $\eta_1=131$ cP for $L1$ and silicone oil for $L2$ ($\eta_2=6.5$ cP). The mean contact angle in this case is $\theta_{12}\approx 70$ deg (Fig. 6(*b*)), which is less than $\pi/2$. Hence, when immersed in a bath of silicone oil, mineral oil partially wets the hydrophilic glass walls. The determination of interfacial tension in a partially wetting situation is often difficult due to contact angle hysteresis. Using the combined capillary rise method, we estimate $\gamma_{12}\approx 0.1$ mN/m for the mineral/silicone oils fluid pair. This extremely low value of γ_{12} falls below the uncertainty of our measurement setup $\Delta\gamma_{12}=0.2$ mN/m. Therefore, this numerical value should be interpreted as an order of magnitude of the interfacial tension between heavy mineral and silicone oils.

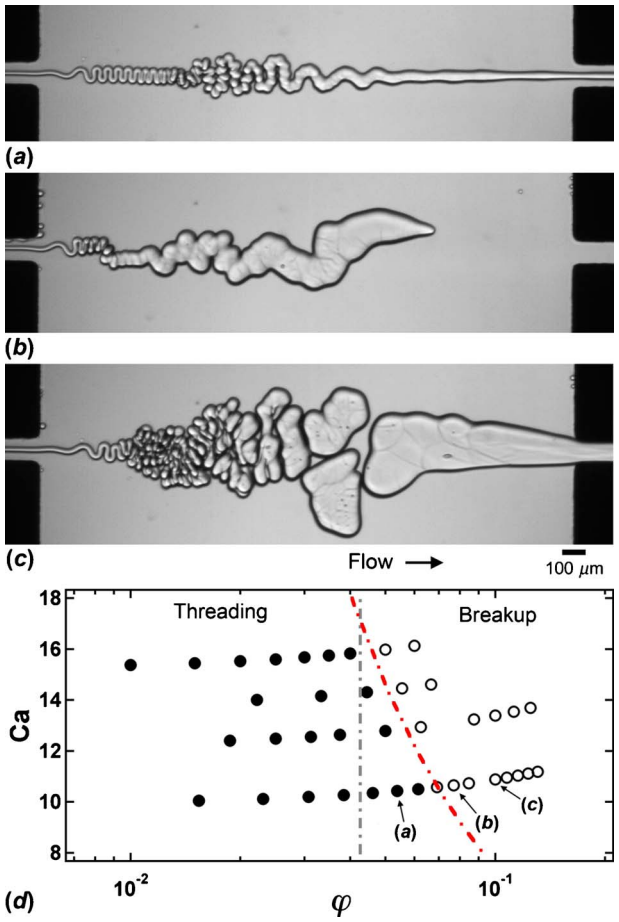

Fig. 7 Deformation of nonwetting threads made of silicone oil in a sheath of ethanol ($\chi=419$). Micrographs of threading and breakup regimes, flow rates in μl/min, $Q_2=130$: (*a*) $Q_1=7$, (*b*) $Q_1=10$, and (*c*) $Q_1=13$. (*d*) Phase-diagram of flow regimes, *Ca* versus φ: threading (●) and breakup (○). Gray dash-dot line: critical flow rate ratio $\varphi_c=0.043$ for the lubrication transition of miscible threads having similar χ. Red dash-dot line: $\varphi_c=0.7Ca^{-1}$.

4.1 Nonwetting Thread. For the case of a nonwetting thread (where $L1$ is made of silicone oil and $L2$ is made of ethanol, contact angle $\theta_{12}\approx 180$ deg, and viscosity ratio $\chi=419$), the presence of a stable thin film of $L2$ at the top and bottom walls of the chamber prevents the lubrication failure of the thread, i.e., the piling regime. Instead, thick threads experience a rather complex breakup process (Fig. 7). In these experiments, the capillary number $Ca=\eta_1(Q_1+Q_2)/(\gamma_{12}h^2)$ is calculated based on the inlet flow in the square microchannel. This quantity allows for nondimensionalizing the flow velocity, which, in contrast with weakly diffusive threads, strongly influences flow morphologies. In the threading regime (Fig. 7(*a*)), a thin capillary thread undergoes primary and secondary folding (i.e., folding of a folded thread).

Primary folds in close proximity coalesce along the flow direction. This mechanism produces a thicker thread having a folding amplitude A, which is gradually damped due to the effects of capillary forces. Therefore, thin threads appear to unfold due to interfacial tension. As φ is increased, the substantial production of fluid interfaces during the buckling of thick capillary threads creates unstable viscous microstructures that subsequently breakup into fluid packets or droplets (Fig. 7(*c*)). The breakup regime is characterized by a succession of states, where widely corrugated threads can either temporary traverse the chamber or breakup. This intriguing "breakup by folding" regime has some direct practical applications since it provides new means for emulsifying high-viscosity fluids at large capillary numbers.

Figure 7(*d*) shows the flow map and transition line between threading and breakup regimes. The critical flow rate ratio φ_c for the transition depends on the capillary number Ca and we empirically find that the function $\varphi_c = 0.7Ca^{-1}$ fits data reasonably well over the range of parameters investigated. This transition can also be roughly estimated based on the fluid viscosity ratio using our previous finding with miscible threads, where $\varphi_c = 1.8\chi^{-0.62}$. Here, for $\chi = 419$, the equivalent critical flow rate ratio for threading/piling would be $\varphi_c = 4.2 \times 10^{-2}$, which appears to asymptotically match data for the threading/breakup transition at large Ca when viscous forces are predominant.

4.2 Partially Wetting Thread. In the situation of a partially wetting thread (where $L1$ is made of heavy mineral oil and $L2$ is made of silicone oil, contact angle $\theta_{12} \approx 70$ deg, and viscosity ratio $\chi = 20$), a variety of forced wetting phenomena are observed during the thread lubrication transition in the cell. This system offers the possibility to examine the competing effects between wetting and encapsulation mechanisms. Indeed, although the large viscosity ratio χ between the fluids facilitates the ensheathing of $L1$ with the formation of a lubricating layer of $L2$ at the walls, the preferred adhesion of $L1$ at the walls can potentially substitute the $L2$ lubricating layer by a $L1$ wetting layer.

An important aspect of wetting phenomena is rooted in the evolution of the dynamic contact angle θ as a function of the capillary number Ca. For a given fluid pair, the advancing contact angle θ_A increases while the receding contact angle θ_R decreases with the contact line velocity [36,37]. Hence, a dynamic wetting transition occurs at the critical capillary number $Ca_c \approx 10^{-2}$ when $\theta_A \to \pi$ and θ_R becomes null [22]. Our microfluidic system, which is composed of a square microchannel with an average velocity $V_{\text{square}} = (Q_1 + Q_2)/h^2$, followed by a plane chamber with an average velocity $V_{\text{chamber}} = (Q_1 + Q_2)/(hw)$, permits the investigation of the crossover between wetting and lubricating regimes. The large reduction in the flow speed between the chamber and the square channel $V_{\text{chamber}} = V_{\text{square}}/20$ is exploited to locally initiate wetting phenomena. However, it is important to note here that since contact lines can align parallel to the mean flow velocity, wetting effects can be observed for $Ca > Ca_c$.

The influence of Ca on flow morphologies is shown in Fig. 8. For low Ca, the combined effect of wetting and interfacial tension causes the thread made of $L1$ to adhere to the walls due to the favorable surface energy. This effect results in the relatively large envelope amplitude A. For larger Ca, viscous effects dominate capillary effects and overall favor the formation of a lubricating layer between the thread and the walls. As the capillary number Ca increases, the folding patterns become more persistent.

We measure the evolution of the normalized thread amplitude A/w as a function of the flow rate ratio φ (Fig. 9). In this series of experiments, we have fixed the side flow rate Q_2 and progressively increased the thread flow rate Q_1 to investigate the transition from a thread to a pile. The relatively smooth relationship between A and φ is expected, given the small viscosity ratio $\chi = 20$ between the fluids. For small and lubricated threads, the amplitude decreases with Ca. By contrast, larger threads readily make direct contact with the walls. The lubrication failure reduces the $L1/L2$ interfacial area and the pile amplitude becomes independent from the capillary number Ca.

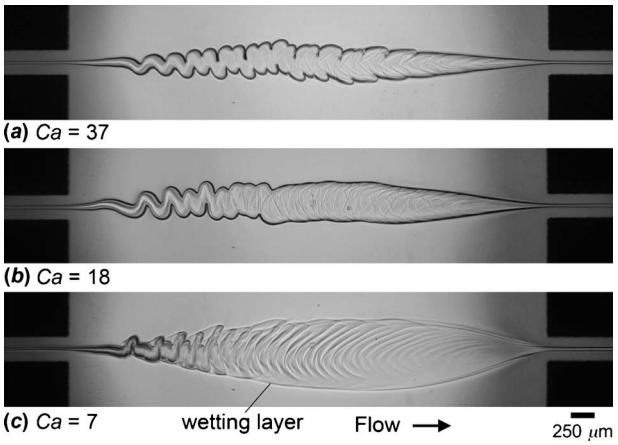

Fig. 8 Influence of capillary number *Ca* and wetting transition for fixed flow rate ratio $\varphi = 5 \times 10^{-2}$ between heavy mineral oil (thread) and silicone oil (sheath). Flow rates in μl/min: (*a*) $Q_1 = 5$, $Q_2 = 100$, and $Ca = 37$, (*b*) $Q_1 = 2.5$, $Q_2 = 50$, and $Ca = 18$, and (*c*) $Q_1 = 1$, $Q_2 = 20$, and $Ca = 7$.

Finally, we focus on the pile morphology for relatively "low" capillary number ($Ca \leq 2.5$) flows (Fig. 10). Here, contact lines are clearly identifiable on the micrographs and interfacial phenomena largely dominate viscous effects, which results in the apparent damping of the folding instability. Although the thread oscillations are significantly reduced, the small variations in the $L2$ film thickness δ are present and develop into small ripples in the center of the pile (Fig. 10(*a*)). The main feature of this regime is the formation and growth of dewetting patches. The interaction between contact angle hysteresis and multifluid flow in the chamber can lead to the formation of pinned contact lines. In these photographs, we visualize contact lines forming both at the top and bottom walls. The nucleation sites of the dewetting patches are located in the slow moving regions of the pile, i.e., in the second half of the chamber near the pile edges. In the absence of external flow, a dewetting patch grows circularly on a homogeneous surface by collecting liquid in a rim near the contact lines [38]. Here, the external flow significantly distorts the patches. Growth of $L1$ patches at the walls is facilitated by the flow in the downstream patch regions while it is hindered in the upstream patch regions since, in this area, the patch growth is against the flow direction. As a result, the system displays the typical morphologies of dewetting arches similar to macroscale systems [39].

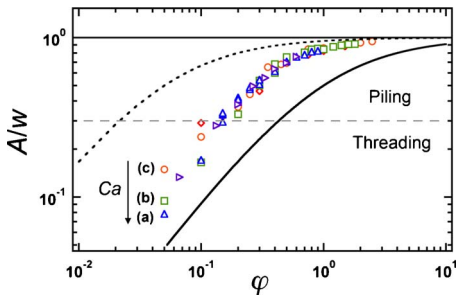

Fig. 9 Evolution of the normalized envelope amplitude *A*/*w* for partially wetting threads as a function of the flow rate ratio φ for various fixed side flow rates (in μl/min) $Q_2 = 10$ (◇), 20 (○), 50 (□), 100 (△), and 150 (▷). (*a*), (*b*), and (*c*) correspond to data in Fig. 8. Solid line: $A/w = [1 + \varphi^{-1}]^{-1}$, dashed-line: $A/w = [1 + \chi\varphi^{-1}]^{-1}$, and gray line: $A/w = 0.3$.

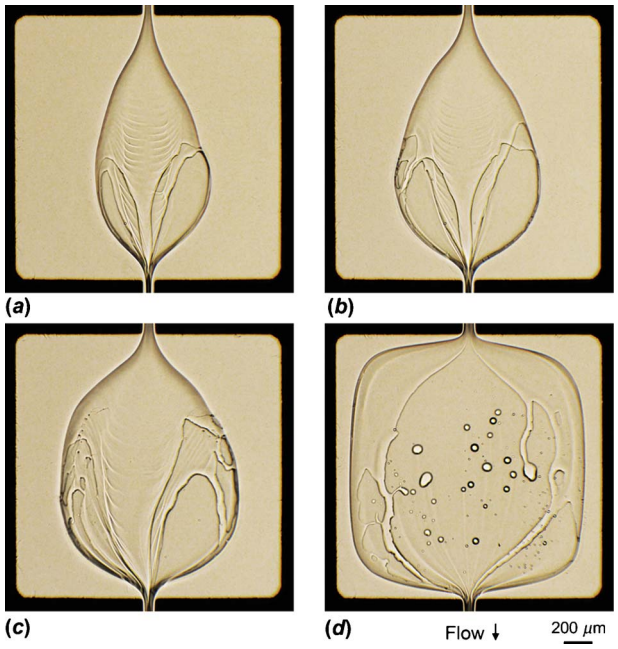

Fig. 10 Dewetting flow patterns between heavy mineral oil (thread) and silicone oil (sheath). Flow rates in μl/min: (*a*) Q_1 =1.5, Q_2=5.4, φ=0.28, and *Ca*=2.4, (*b*) Q_1=1.5, Q_2=4, φ=0.37, and *Ca*=1.9, (*c*) Q_1=1.5, Q_2=3, φ=0.5, and *Ca*=1.6, and (*d*) Q_1 =5, Q_2=2, φ=2.5, and *Ca*=2.5.

For intermediate pile amplitude A, since contact lines have a tendency to align with the flow, we observe the formation of rivulets (i.e., continuous fingers) in the central region. For larger A, most of the pile is dewetted (Fig. 10(*d*)) and droplets of $L2$ can stick to the walls in the center of the pile. This phenomenon is closely related to the stability of rivulets that can break into an assembly of droplets when not "fed" by $L2$.

5 Conclusions

In this paper, we have discussed the lubrication transition of viscous threads in a microfluidic chamber for both miscible and immiscible environments. The single-phase flow streamlines in a quasi-two-dimensional cell can be approximated by arc of circles in the center of the chamber. Weakly diffusive viscous core-annular flows experience a dramatic lubrication failure as a function of the flow rates Q_1 and Q_2 and the viscosity ratio $\chi = \eta_1/\eta_2$. This transition can be predicted using a simple estimate for the critical flow rate ratio φ_c as a function of χ. In addition, we have characterized the amplitude of the folding envelope in the threading regime and introduced geometric parameters for analyzing the pile morphology. When fluids are immiscible, the behavior of capillary threads in the nonwetting and partially wetting cases is examined. A thin nonwetting thread can unfold due to capillary effects while a thick thread can breakup due to the combination of viscous and capillary instabilities. A partially wetting thread exhibits a complex behavior depending on contact angle hysteresis. Although the fluid pair (mineral/silicone oils) used in this experiment has an extremely low interfacial tension, fluid contact lines appear clearly at the walls, which is in contrast with purely miscible fluid systems. A regime of particular interest corresponds to the formation and growth of dewetting patches between the liquids and the walls.

Better understanding of core-annular flow regimes yields insight into novel flow configurations of both fundamental and practical interests. Here, we have investigated the degree of deformation that such structures can sustain in a two-dimensional cell primarily as a function of the viscosity ratio. The quantification of the film thickness δ at the walls in both miscible and immiscible cases should yield significant insights on the lubrication transition of deformed threads. Numerical simulations and theoretical stability analysis of these emerging phenomena would shed new light into the complex interplay between thread encapsulation and wetting properties. Controlling the lubrication of fluids having a large difference in viscosity is pivotal for the development of novel microflow reactors for soft materials.

Acknowledgment

This material is based on work supported by the National Science Foundation under Grant No. CBET-0932925.

Nomenclature

A = envelope amplitude
c = constant
Ca = capillary number in the square channel based on the inlet flow
Ca_1 = capillary number associated with the injection flow rate of the more viscous fluid
Ca_c = critical capillary number
D = molecular diffusion coefficient
h = channel height
k = prefactor
$L1$ = more viscous liquid (core liquid)
$L2$ = less viscous liquid (sheath liquid)
Pe = Péclet number
Q_1 = flow rate associated with $L1$
Q_2 = flow rate associated with $L2$
r = radial distance from the source
V = average flow velocity
V_{chamber} = average velocity in the chamber
V_{square} = average velocity in the square channel
w = channel width
X_M = location of the maximum amplitude
X_P = penetration length of the lubricated thread into the pile

Greek Letters

α = streamline initial angle
χ = viscosity ratio
δ = $L2$ film thickness
ε = thread diameter in the square channel
ε_c = critical thread size
γ = shear rate
γ_{12} = interfacial tension between $L1$ and $L2$
$\Delta\gamma_{12}$ = uncertainty in interfacial tension measurement
η = viscosity
η_1 = viscosity associated with $L1$
η_2 = viscosity associated with $L2$
φ = flow rate ratio between $L1$ and $L2$
φ_c = critical flow rate ratio
θ = dynamic contact angle
θ_{12} = contact angle between $L1$ and $L2$
θ_A = advancing contact angle
θ_R = receding contact angle

References

[1] Ho, C.-M., and Tai, Y.-C., 1998, "Micro-Electro-Mechanical Systems (MEMS) and Fluid Flows," Annu. Rev. Fluid Mech., **30**, pp. 579–612.
[2] Stone, H. A., Stroock, A. D., and Ajdari, A., 2004, "Engineering Flows in Small Devices: Microfluidics Toward a Lab-on-a-Chip," Annu. Rev. Fluid Mech., **36**, pp. 381–411.
[3] Squires, T. M., and Quake, S. R., 2005, "Microfluidics: Fluid Physics at the Nanoliter Scale," Rev. Mod. Phys., **77**, pp. 977–1026.
[4] Yager, P., Edwards, T., Fu, E., Helton, K., Nelson, K., Tam, M. R., and Weigl, B. H., 2006, "Mirofluidic Diagnostic Technologies for Global Public Health," Nature (London), **442**, pp. 412–418.
[5] deMello, A. J., 2006, "Control and Detection of Chemical Reactions in Microfluidic Systems," Nature (London), **442**, pp. 394–402.

[6] El-Ali, J., Sorger, P. K., and Jensen, K. F., 2006, "Cells on Chips," Nature (London), **442**, pp. 403–411.
[7] Craighead, H., 2006, "Future Lab-on-Chip Technologies for Interrogating Individual Molecules," Nature (London), **442**, pp. 387–393.
[8] Meng, D. D., Cubaud, T., Ho, C.-M., and Kim, C.-J., 2007, "A Methanol-Tolerant Gas-Venting Microchannel for Microdirect Methanol Fuel Cell," J. Microelectromech. Syst., **16**, pp. 1403–1410.
[9] Wolfe, D. B., Conroy, R. S., Garstecki, P., Mayer, B. T., Fischbach, M. A., Paul, K. E., Pretiss, M., and Whitesides, G. M., 2004, "Dynamic Control of Liquid-Core/Liquid-Cladding Optical Waveguides," Proc. Natl. Acad. Sci. U.S.A., **101**, pp. 12434–12438.
[10] Mao, X., Waldeisen, J. R., Juluri, B. K., and Huang, T. H., 2007, "Hydrodynamically Tunable Optofluidic Cylindrical Microlens," Lab Chip, **7**, pp. 1303–1308.
[11] Tang, S. K. Y., Stan, C. A., and Whitesides, G. M., 2008, "Dynamically Reconfigurable Liquid-Core Liquid-Cladding Lens in a Microfluidic Channel," Lab Chip, **8**, pp. 395–401.
[12] Song, H., Chen, D. L., and Ismagilov, R. F., 2006, "Reactions in Droplets in Microfluidic Channels," Angew. Chem., Int. Ed., **45**, pp. 7336–7356.
[13] Teh, S. Y., Lin, R., Hung, L. H., and Lee, A. P., 2008, "Droplet Microfluidics," Lab Chip, **8**, pp. 198–220.
[14] Günther, A., and Jensen, K. F., 2006, "Multiphase Microfluidics: From Flow Characteristics to Chemical and Materials Synthesis," Lab Chip, **6**, pp. 1487–1503.
[15] Kawakatsu, T., Komori, H., Nakajima, M., Kikuchi, Y., and Yonemoto, T., 1999, "Production of Monodisperse Oil-in-Water Emulsion Using Cross Flow-Type Silicon Microchannel Plate," J. Chem. Eng. Jpn., **32**, pp. 241–244.
[16] Anna, S. L., Bontoux, N., and Stone, H. A., 2003, "Formation of Dispersions Using "Flow Focusing" in Microchannels," Appl. Phys. Lett., **82**, pp. 364–366.
[17] Xu, Q., and Nakajima, M., 2004, "The Generation of Highly Monodisperse Droplets Through the Breakup of Hydrodynamically Focused Microthread in a Microfluidic Device," Appl. Phys. Lett., **85**, pp. 3726–3728.
[18] Cubaud, T., Tatineni, M., Zhong, X., and Ho, C.-M., 2005, "Bubble Dispenser in Microfluidic Devices," Phys. Rev. E, **72**, p. 037302.
[19] Garstecki, P., Fuerstman, M., Stone, H. A., and Whitesides, G. W., 2006, "Formation of Droplets and Bubbles in a Microfluidic T-Junction-Scaling and Mechanism of Breakup," Lab Chip, **6**, pp. 437–449.
[20] Utada, A. S., Fernandez-Nieves, A., Stone, H. A., and Weitz, D. A., 2007, "Dripping to Jetting Transitions in Coflowing Liquid Streams," Phys. Rev. Lett., **99**, p. 094502.
[21] Cubaud, T., and Mason, T. G., 2006, "Folding of Viscous Threads in Diverging Microchannels," Phys. Rev. Lett., **96**, p. 114501.
[22] Cubaud, T., and Mason, T. G., 2008, "Capillary Threads and Viscous Droplets in Square Microchannels," Phys. Fluids, **20**, p. 053302.
[23] Cubaud, T., and Mason, T. G., 2009, "High-Viscosity Fluid Threads in Weakly Diffusive Microfluidic Systems," New J. Phys., **11**, p. 075029.
[24] Joseph, D. D., Nguyen, K., and Beavers, G. S., 1984, "Non-Uniqueness and Stability of the Configuration of Flow of Immiscible Fluids With Different Viscosities," J. Fluid Mech., **141**, pp. 319–345.
[25] Joseph, D. D., and Renardy, Y. Y., 1993, *Fundamentals of Two-Fluid Dynamics. Part II: Lubricated Transport, Drops and Miscible Liquids*, Springer-Verlag, New York.
[26] Landau, L. D., and Lifshitz, E. M., 1986, *Theory of Elasticity*, Pergamon, Oxford.
[27] Buckmaster, J. D., 1973, "The Buckling of Thin Viscous Jets," J. Fluid Mech., **61**, pp. 449–463.
[28] Maleki, M., Habibi, M., Golestanian, R., Ribe, N. M., and Bonn, D., 2004, "Liquid Rope Coiling on a Solid Surface," Phys. Rev. Lett., **93**, p. 214502.
[29] Koulakis, J. P., Mitescu, C. D., Brochard-Wyart, F., de Gennes, P. G., and Guyon, E., 2008, "The Viscous Catenary Revisited: Experiments and Theory," J. Fluid Mech., **609**, pp. 87–110.
[30] Cubaud, T., and Ho, C.-M., 2004, "Transport of Bubbles in Square Microchannels," Phys. Fluids, **16**, pp. 4575–4585.
[31] Gondret, P., and Rabaud, M., 1997, "Shear Instability of Two-Fluid Parallel Flow in a Hele–Shaw Cell," Phys. Fluids, **9**, pp. 3267–3274.
[32] Batchelor, G. K., 1967, *An Introduction to Fluid Mechanics*, Cambridge University Press, New York.
[33] Cubaud, T., and Mason, T. G., 2007, "A Microfluidic Aquarium," Phys. Fluids, **19**, p. 091108.
[34] Cubaud, T., and Mason, T. G., 2008, "Formation of Miscible Fluid Microstructures by Hydrodynamic Focusing in Plane Geometries," Phys. Rev. E, **78**, p. 056308.
[35] Rashidnia, N., Balasubramaniam, R., and Del Signore, D., 1992, "Interfacial Tension Measurement of Immiscible Liquids Using a Capillary Tube," AIChE J., **38**, pp. 615–618.
[36] Le Grand, N., Daerr, A., and Limat, L., 2005, "Shape and Motion of Drops Sliding Down in Inclined Plane," J. Fluid Mech., **541**, pp. 293–315.
[37] Snoeijer, J. H., Delon, G., Fermigier, M., and Andreotti, B., 2006, "Avoided Critical Behavior in Dynamically Forced Wetting," Phys. Rev. Lett., **96**, p. 174504.
[38] Redon, C., Brochard-Wyart, F., and Rondelez, F., 1991, "Dynamics of Dewetting," Phys. Rev. Lett., **66**, pp. 715–718.
[39] Rio, E., and Limat, L., 2006, "Wetting Hysteresis of a Dry Patch Left Inside a Flowing Film," Phys. Fluids, **18**, p. 032102.